Tailoring wall permeabilities for enhanced filtration

J. G. Herterich, D. Vella, R. W. Field, N. P. Hankins, and I. M. Griffiths

Citation: Physics of Fluids (1994-present) **27**, 053102 (2015); doi: 10.1063/1.4919658
View online: http://dx.doi.org/10.1063/1.4919658
View Table of Contents: http://scitation.aip.org/content/aip/journal/pof2/27/5?ver=pdfcov
Published by the AIP Publishing

PHYSICS OF FLUIDS **27**, 053102 (2015)

Tailoring wall permeabilities for enhanced filtration

J. G. Herterich,[1] D. Vella,[1] R. W. Field,[2] N. P. Hankins,[2] and I. M. Griffiths[1,a)]
[1]*Mathematical Institute, University of Oxford, Radcliffe Observatory Quarter, Oxford OX2 6GG, United Kingdom*
[2]*Department of Engineering Science, University of Oxford, Oxford OX1 3PJ, United Kingdom*

(Received 6 December 2014; accepted 18 April 2015; published online 12 May 2015)

The build-up of contaminants at the wall of cross-flow membrane filtration systems can be detrimental to the operation of such systems because of, amongst other things, the osmotic backflow it may induce. In this paper, we propose a strategy to avoid the negative effects of backflow due to osmosis by using 2D channels bounded by walls with a combination of permeable and impermeable segments. We show that preventing flow through the final portion of the channel can increase the efficiency of filtration and we determine the optimal fraction occupied by the permeable wall that maximizes efficiency. Our analysis uses a combination of numerical techniques and asymptotic analysis in the limit of low wall permeabilities. Finally, we consider how the energy cost of filtration depends on the Péclet number and show that the energy cost per unit of filtered water may be minimized by appropriately choosing both the Péclet number and the permeable-region fraction. © *2015 AIP Publishing LLC*. [http://dx.doi.org/10.1063/1.4919658]

I. INTRODUCTION

An important area of increasing interest in science and engineering is the filtration of contaminated water to produce clean, potable water. Contaminated water is, at its simplest, a suspension of particles and other contaminants in water, and so fluid mechanics plays an important role in filtration. One of the most common forms of water filtration is cross-flow membrane filtration.[1,2] The fluid-mechanical principles underlying cross-flow filtration are relatively simple: particle-laden water enters a specially designed module (that we take to have the shape of a channel) with permeable walls that allow the fluid, but not the suspended particles, to pass through to the permeate side. The fluid flows towards the walls as well as along the channel, advecting particles towards the walls. This build-up of particles is moderated by diffusion towards the centre of the channel. The resulting particle concentration profile, higher at the walls than the centre, exhibits what is known as concentration polarization (CP).[3,4] There are many adverse effects of concentration polarization, including a greater propensity for blockage of the membrane pores, restricting flow through the permeable walls,[5] as well as an increased osmotic pressure,[6] which acts to draw clean water into the channel, reducing filtration performance (Figure 1).

There has been extensive mathematical modelling of concentration polarization in boundary layers at a permeable wall. The convection–diffusion of particles in a steady-state boundary layer with concentration-dependent viscosity and diffusivity given in Refs. 7 and 8 has been studied, giving rise to similarity solutions. Other papers in the literature aim to unify different aspects of filtration of colloidal particles such as concentration polarization and deposition.[9] These models assume that outside the boundary layer the bulk concentration of particles is constant. This common assumption in the literature may be achieved by a large Péclet number.

Some previous works have focused on the effect of manipulating the fluid flow, for example, by increasing shear rate[6] or vortex mixing,[10] as well as many other methods,[11,12,30] to remove

a)Author to whom correspondence should be addressed. Electronic mail: ian.griffiths@maths.ox.ac.uk

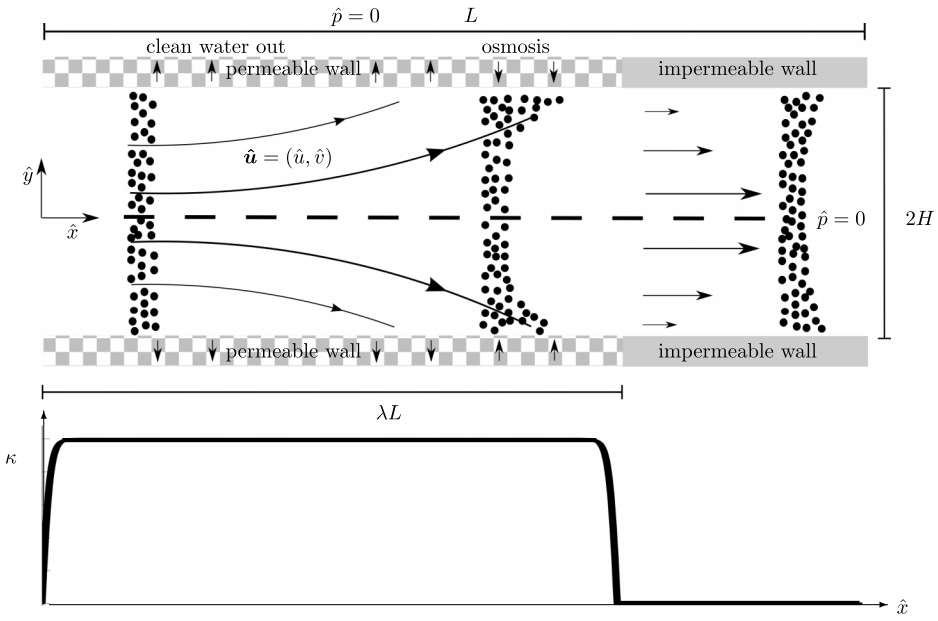

FIG. 1. Above: schematic of a channel containing a suspension of particles. The suspension enters from the left and flows along the channel. The walls are a permeable membrane for a section of the channel and impermeable towards the end of the channel, as depicted in the sketch of the effective permeability, κ, of the channel (below). Particles are advected towards the wall by the flow, increasing the osmotic pressure at the walls, and diffuse back into the channel when the walls are impermeable. If the osmotic pressure exceeds the fluid pressure, osmosis occurs. In the impermeable-walled region, there is no flow through the walls.

particles from the wall. These may involve a structural change to the channel, such as furrowed or dimpled wall surfaces to produce the vortex mixing, resulting in complicated fluid flows. Here, we consider low Reynolds numbers flows and impose a structural change to the channel that does not overcomplicate the flow. This structural change is to alter the wall permeability to block that part of the porous wall that may otherwise result in high osmotic pressures that draw fluid into the channel from the permeate side. Operating in a slow flow regime results in a greater deposition of particles at the membrane surface.[13] Although we do not consider deposition, the concentration polarization observed represents the early stages of particle build-up that may ultimately lead to deposition and cake formation.

We consider a membrane filtration system with a flow from left to right induced by a pressure gradient (Figure 1). Membrane filtration systems utilize a higher fluid pressure to overcome the osmotic pressure, ensuring sustained water filtration. The rationale for altering the wall permeabilities stems from considering the hydrodynamic pressure within a channel with walls of uniform permeability. Fluid leaks out of the wall (leaving particles behind) at a rate, $\hat{\mathcal{V}}$, that depends on the overall effective transmembrane pressure difference, $\Delta\hat{p} - \Delta\hat{\pi}$, where $\Delta\hat{p}$ is the difference between the hydrodynamic pressure in the channel at the wall and the pressure outside the channel and $\Delta\hat{\pi}$ is the osmotic pressure difference across the permeable membrane wall.[1,6] Motivated by Darcy's law, we write

$$\hat{\mathcal{V}} = \hat{\kappa}(\Delta\hat{p} - \Delta\hat{\pi}), \tag{1}$$

where $\hat{\kappa} = k/\mu b$ is the spatially varying effective permeability, related to the wall permeability, k, fluid viscosity, μ, and wall thickness, b. (The form of Eq. (1) may also be justified more rigorously from arguments based on irreversible thermodynamics.[14,15]) We assume that the filter is perfect, i.e., complete rejection of particles occurs at the channel wall. If the osmotic pressure exceeds the fluid pressure, then the flow is reversed and clean water flows into the channel, a process we call *backflow*.

Backflow of clean water into the channel is very inefficient for the filtration process; energy has been used in extracting the clean water, only for it to re-enter the contaminated flow. Since the region most prone to this osmotic backflow is the end (where $\Delta\hat{p}$ is smallest), it is natural to consider whether replacing the permeable wall with an impermeable wall in this region would eliminate the backflow. However, the size of this impermeable region needs to be carefully chosen: too short and backflow will still occur, too long and there is insufficient opportunity for clean water to flow out. Both of these scenarios compromise filtration efficiency. For example, consider a system with permeable walls throughout, with constant pressure gradient, and a constant osmotic pressure. Equation (1) implies that filtration occurs when $\hat{p} > \hat{\pi}$, and backflow occurs when $\hat{\pi} > \hat{p}$ (Figure 2(a)). If we set the permeability to be zero beyond a certain point in the channel (ignoring the changes this will induce in the pressure for this illustrative example), then the region where backflow by osmosis was previously active has been modified so that this no longer occurs and thus, the amount of net fluid filtered is increased (Figure 2(b)).

For simplicity, we take the fluid pressure at the end of the channel to be equal to the fluid pressure outside the channel (on the permeate side of the permeable wall). At the outlet, the hydrodynamic pressure difference across the membrane is then zero, and as a result, any non-zero osmotic pressure difference near the end of the channel will result in a backflow (see Eq. (1)). We note that simply shortening the channel will not remedy this inevitable flow reversal (since wherever the end is open, the pressure difference is zero). An alternative approach would be to take a positive reference pressure at the end of the channel and/or a negative reference outer pressure, as explored in Ref. 16. However, keeping these additional pressure differences in place during operation in a membrane filtration device may require additional energy. Our proposed setup of partially blocking the end of the device offers a simple way of resolving this issue.

Energy cost is an important consideration for filtration devices. The input energy is required for pumping the flow and creating the pressure in the filtration device. Although the volume filtered increases with cross-flow velocity, the power requirement for the pump can increase by as much as the cube of the cross-flow velocity.[17] This results in a trade-off between input energy and filtration output.

In this paper, we examine the advantages of using a spatially varying wall permeability in order to optimize the efficacy of filtration. We examine in detail, using numerical and asymptotic techniques, a channel that has a permeable region followed by an impermeable region to illustrate the significant effect that backflow due to osmosis can have on a system where the hydrodynamic pressure and osmotic pressure are of the same order of magnitude. We also consider the impact of a variable permeability on the energy cost for filtration.

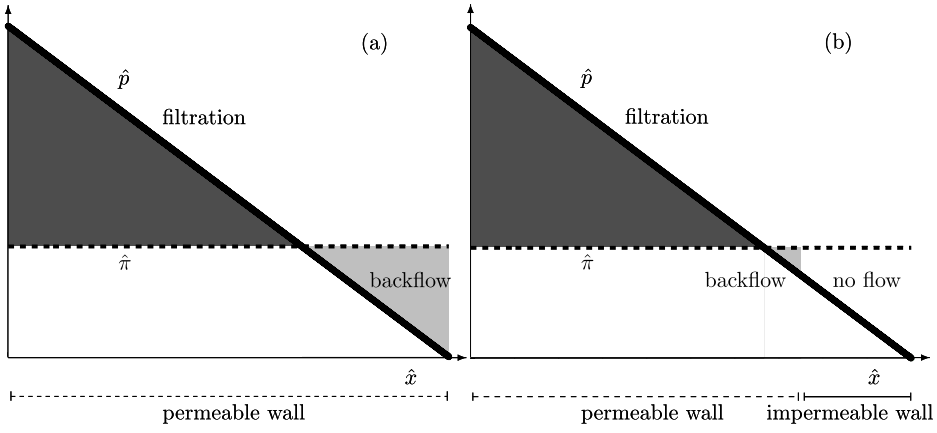

FIG. 2. Schematic showing the hydrodynamic pressure (solid black), $\hat{p}$, and osmotic pressure (dashed black), $\hat{\pi}$, as functions of the distance along the channel. The sign of $\hat{p}-\hat{\pi}$ determines whether filtration (dark grey) or backflow (light grey) occurs. (a) For a spatially uniform permeability, the effect of backflow significantly decreases the efficiency of filtration. (b) Introducing an impermeable region (no flow, white) reduces backflow and increases net filtration.

II. MATHEMATICAL MODELLING

We model the input fluid as a dilute suspension of neutrally buoyant small particles, typically tens of nanometres in radius. The fluid flows into a 2D channel of length L, at a controlled rate with areal flux $2\hat{Q}$. The walls of the channel are positioned at $\hat{y} = \pm H$ (Figure 1). The walls comprise a region of uniform non-zero permeability followed by a region that is impermeable. On the outside of the channel, and at the end of the channel ($\hat{x} = L$), the fluid pressure is constant; we take this value to be our pressure datum. Upon entering the channel, the suspension is advected down the channel and towards the permeable walls; at the wall, the suspended particles are rejected allowing only clean water to flow out. The rate at which clean fluid (the permeate) flows through the permeable walls is proportional to the effective transmembrane pressure difference, as seen in Eq. (1). Fluid that does not pass through the walls, together with the rejected particles (forming the retentate), leaves the channel at the open end, $\hat{x} = L$. We consider the steady-state (time-independent) operation of the system.

For suspensions with large volume fractions, both the fluid viscosity, μ, and particle diffusivity, D, will be significantly altered by the presence of particles. For simplicity however, and to highlight the fundamental aspects of this problem, we neglect such effects taking μ and D to be constant, as is the case for dilute suspensions.[16,18] To estimate the typical parameters of filtration, we consider values representative of cross-flow filtration of small particles such as viruses, as considered in Ref. 19. In these systems, the virus particles are typically tens of nanometres in radius. For hollow fibre membrane modules, the membrane channels are separated by 200 μm with a tangential flow at a shear rate of 1200 s^{-1} (Ref. 19) corresponding to a typical flow speed, U, that is of order tens of centimetres per second. Typical membrane channels have length $L \sim 1$ m and width $H \sim 200$ μm.[20] Hence the aspect ratio, $\delta = H/L = 2 \times 10^{-4} \ll 1$; we shall exploit this small aspect ratio in our analysis. The density and viscosity of water are $\rho = 1000$ kg/m^3 and $\mu \sim 1$ mPa s, respectively, and the diffusion constant, $D \sim 10^{-11}$ m^2/s, by the Stokes–Einstein relation.[21] The reduced Reynolds number, $\mathrm{Re} = \delta^2 \rho U L/\mu \sim 10^{-3}$ is small, so inertial forces may be neglected. The reduced Péclet number, $\mathrm{Pe} = \delta^2 UL/D \sim 10^2$, is rather large. However, we appreciate that $\delta\,\mathrm{Pe}$ is small so that Pe is not a large number for a thin-channel flow. A smaller-order Péclet number may be achieved by a slower flow, of order cm/s.[20] As such, we will assume an order-one Péclet number as operating under this condition allows for the richest particle dynamics in the channel. From a Stokes-equation scaling for pressure in a channel, the fluid pressure scales like $P = \mu U/\delta^2 L \sim 10^3$ Pa. The typical osmotic pressure, Π, is given by the Morse equation[22,23] for a dilute suspension of particles, $\Pi = iRT/N_A V^*$. Here, i is the van't Hoff factor providing a measure of the effect of the solute on various colligative properties of the solution ($i = 1$ for viruses), $R = 8.314$ J/mol K is the gas constant, T the absolute temperature (taken to be room temperature $\approx$300 K). Avogadro's number, N_A, and the volume of a single contaminant particle, $V^* = 4\pi a^3/3$ m^3, where a is the particle size of tens of nanometers, play a role via the conversion from density to volume fraction. Hence, $\Pi \sim 10^3$ Pa is the same order as the fluid pressure.

A. Governing equations

As we have a small reduced Reynolds number, the fluid flow, $\hat{\boldsymbol{u}} = (\hat{u}, \hat{v})$, is governed by the steady Stokes equations, representing conservation of mass and momentum of the fluid,

$$\boldsymbol{\nabla} \cdot \hat{\boldsymbol{u}} = 0, \tag{2a}$$

$$\mu \boldsymbol{\nabla}^2 \hat{\boldsymbol{u}} = \boldsymbol{\nabla} \hat{p}, \tag{2b}$$

where $\hat{p}$ is the fluid pressure. The particle volume fraction, $\hat{\phi}$, is governed by the steady advection–diffusion equation

$$\hat{\boldsymbol{u}} \cdot \boldsymbol{\nabla} \hat{\phi} = D\, \boldsymbol{\nabla}^2 \hat{\phi}. \tag{3}$$

B. Boundary conditions

We assume that the particles enter the channel uniformly distributed over the cross-section,

$$\hat{\phi}(0, \hat{y}) \equiv \Phi_0, \tag{4}$$

where Φ_0 is a constant.

We assume that the fluid flow and particle concentration are symmetric about the x-axis of the channel, that is,

$$\frac{\partial \hat{\phi}}{\partial \hat{y}} = \frac{\partial \hat{u}}{\partial \hat{y}} = \hat{v} = 0 \quad \text{on} \quad \hat{y} = 0, \tag{5}$$

and so we need only consider the behaviour in the half-channel $0 \le \hat{y} \le H$.

The fluid flow through the (permeable) channel walls is given by

$$\hat{v}(\hat{x}, H) = \hat{\mathcal{V}}(\hat{x}) = \hat{\kappa}(\hat{x})(\Delta\hat{p} - \Delta\hat{\pi}) \tag{6}$$

on $\hat{y} = H$ as in Eq. (1), where $\hat{\kappa}(\hat{x})$ is the spatially varying effective permeability to be specified later, $\Delta\hat{p}(\hat{x}, H) = \hat{p} - \hat{p}_{\text{outer}}$ is the difference between the hydrodynamic pressure in the channel at the wall and the pressure outside the channel, $\hat{p}_{\text{outer}}$ (assumed constant). We assume that the end of the channel is open so that the pressure at the outlet $\hat{p}_{\text{end}} = \hat{p}_{\text{outer}}$. Since the system is driven only by pressure differences, the choice we then make for this outer pressure does not affect the system behavior. Similarly, $\Delta\hat{\pi} = \hat{\pi} - \hat{\pi}_{\text{outer}}$ is the osmotic pressure difference across the wall where $\hat{\pi}$ is the osmotic pressure due to particles in the channel and $\hat{\pi}_{\text{outer}}$ is that due to contaminants outside the channel. Assuming complete rejection of particles at the channel wall, i.e., a perfect filter, we take $\hat{\pi}_{\text{outer}} = 0$. The osmotic pressure is, in general, a function of the volume fraction of particles at the surface of the permeable wall,

$$\hat{\pi}(x)|_{\hat{y}=H} = \Pi\Phi_0\, \hat{\phi}(\hat{x}, \hat{y} = H). \tag{7}$$

In general, at a permeable wall there is a tangential *slip velocity*, whose magnitude is determined by a Neumann boundary condition such as that given in Ref. 24. However, it has been found that this slip is not significant for a wide range of membranes,[25,26] and so here, for simplicity, we shall assume a no-slip boundary condition

$$\hat{u}(\hat{x}, H) = 0, \tag{8}$$

as also adopted in Ref. 27.

Since particles are completely rejected by the wall, we apply the no-flux boundary condition[7,9]

$$\hat{\mathcal{V}}\hat{\phi} - D\frac{\partial \hat{\phi}}{\partial \hat{y}} = 0 \quad \text{on} \quad \hat{y} = H. \tag{9}$$

In general, the inlet condition (4) will not satisfy this boundary condition. However, a small boundary layer region is present in which the concentration appropriately adjusts. At the inlet, we impose a constant inlet flow, $2\hat{Q}$,

$$2\hat{Q} = \int_{-H}^{H} \hat{u}\, \mathrm{d}\,\hat{y} = 2\int_{0}^{H} \hat{u}\, \mathrm{d}\,\hat{y} \quad \text{at} \quad \hat{x} = 0. \tag{10}$$

The above boundary conditions will suffice as we will consider a thin-channel approximation in Sec. II C that reduces the order of the problem.

From a practical point of view, the amount of fluid filtered through the walls,

$$\hat{F} = 2\int_{0}^{L} \hat{\mathcal{V}}\, \mathrm{d}\,\hat{x}, \tag{11}$$

is of interest.

C. Non-dimensionalization and thin-channel approximation

Since our system is dependent on the competing forces of hydrodynamic pressure and osmotic pressure, and we have shown these to be of the same order for our system, it is natural to scale $\hat{p}$ and $\hat{\pi}$ in the same way; Eq. (7) indicates that the natural scaling choice is $\Pi\Phi_0$; L and $H = \delta L$ are used to non-dimensionalize lengths as appropriate. We thus let

$$\begin{aligned} \hat{x} &= Lx, & \hat{y} &= \delta L y, & \hat{\phi} &= \phi, & \hat{\pi} &= \Pi\Phi_0\pi, \\ \hat{u} &= \frac{\hat{Q}}{\delta L}u, & \hat{v} &= \frac{\hat{Q}}{L}v, & \hat{p} &= \Pi\Phi_0 p + \hat{p}_{\text{outer}}, & \hat{\kappa} &= \frac{D}{\Pi\Phi_0\delta L}\kappa, \end{aligned} \tag{12}$$

where the scalings of u, v arise in order to balance the equations and to eliminate $\hat{Q}$ from the influx condition. Hence, the earlier defined velocity scale is $U = \hat{Q}/\delta L$. Substituting scalings (12) into Eqs. (2) and (3), and retaining only leading-order terms in $\delta \ll 1$, provides the governing equations for the system,

$$\frac{\partial u}{\partial x} + \frac{\partial v}{\partial y} = 0, \tag{13a}$$

$$\mathrm{Pe}\mathcal{D}\frac{\partial^2 u}{\partial y^2} = \frac{\partial p}{\partial x}, \tag{13b}$$

$$0 = \frac{\partial p}{\partial y}, \tag{13c}$$

$$\mathrm{Pe}\left(u\frac{\partial \phi}{\partial x} + v\frac{\partial \phi}{\partial y}\right) = \frac{\partial^2 \phi}{\partial y^2}, \tag{13d}$$

for $0 \le x \le 1$ and $0 \le y \le 1$ with the channel walls at $y = \pm 1$ (with symmetry about $y = 0$). Here, $\mathrm{Pe} = \delta\hat{Q}/D$ is the reduced Péclet number, a measure of the ratio of advection to diffusion of the particles in a thin channel, and $\mathcal{D} = \mu D/\delta^4 L^2 \Pi\Phi_0$ is a dimensionless number. We note that $1/\mathcal{D} = b(\delta^4 L^2 \Pi\Phi_0/\mu b)/D$, so that $\mathcal{D}$ is identified as an inverse Péclet number where the velocity scale is the Darcy velocity across a membrane of thickness b with permeability scaling like a length squared, $\delta^4 L^2$. Hence, $\mathrm{Pe}\mathcal{D}$ represents a ratio of Péclet numbers. By our parameter estimations, $\mathrm{Pe}\mathcal{D}$ is an order-one quantity. Throughout this paper, we take the Péclet number to be an order-one quantity as this regime produces the richest dynamics. The influx, $\hat{Q}$, that has been scaled out of the problem appears in the Péclet number. This affects the fluid flow in Eq. (13b), and the particles in Eq. (13d).

Note that there is no axial diffusion term in the leading-order advection–diffusion equation (13d) due to the thin-channel approximation ($\delta \ll 1$). The y-momentum equation (13c) indicates that the pressure is a function of x only, i.e., $p = p(x)$, as is familiar from lubrication theory and other thin-layer models of fluid flow. Furthermore, our non-dimensionalization means that the osmotic pressure at the walls from Eq. (15c) now reads

$$\pi(x) = \phi_w(x), \tag{14}$$

where we have introduced $\phi_w(x) = \phi(x, y = 1)$ to denote the particle concentration at the wall.

The dimensionless boundary conditions read

$$\text{symmetry :} \quad \frac{\partial \phi}{\partial y} = \frac{\partial u}{\partial y} = v = 0, \quad \text{on } y = 0, \tag{15a}$$

$$\text{no axial wall slip:} \quad u = 0, \quad \text{on } y = 1, \tag{15b}$$

$$\text{permeate flow:} \quad \mathcal{V} = \frac{\kappa(x)}{\mathrm{Pe}}(p - \phi_w), \quad \text{on } y = 1, \tag{15c}$$

$$\text{perfect filtering of particles:} \quad \mathrm{Pe}\,\mathcal{V}\,\phi - \frac{\partial \phi}{\partial y} = 0, \quad \text{on } y = 1, \tag{15d}$$

$$\text{fluid influx:} \quad \int_0^1 u\,\mathrm{d}y = 1, \quad \text{at } x = 0, \tag{15e}$$

fixed outlet pressure: $p = 0,$ at $x = 1,$ (15f)

inlet condition: $\phi \equiv 1,$ at $x = 0.$ (15g)

The influx, $\hat{Q}$, appears through the Péclet number in the boundary conditions, affecting the flow in Eq. (15c) and the particles in Eq. (15d). This non-dimensionalization results in four free parameters: the Péclet number, Pe, the permeability, κ, the permeable wall fraction, λ, and a dimensionless number, $\mathcal{D}$. In Sec. III, we fix $\mathcal{D} = 1$ and investigate the effects of varying λ with each of κ and Pe in turn.

D. Solution of flow problem

The system of equations (13a) and (13b) with boundary conditions (15a) and (15b) can be solved immediately to give the flow within the channel. The axial and transverse velocities are given by

$$u(x, y) = \frac{1}{\mathrm{Pe}\mathcal{D}} \frac{\mathrm{d}p}{\mathrm{d}x} \frac{y^2 - 1}{2}, \tag{16a}$$

$$v(x, y) = \frac{1}{\mathrm{Pe}\mathcal{D}} \frac{\mathrm{d}^2 p}{\mathrm{d}x^2} \frac{3y - y^3}{6}, \tag{16b}$$

respectively, where the factor $1/\mathrm{Pe}\mathcal{D}$ represents the scaling for the ratio of Péclet numbers. This is a classic result and can be found in many textbooks.[28]

The hydrodynamic pressure in the channel is then determined by boundary condition (15c) and Eq. (16b), resulting in an ordinary differential equation (ODE) for p,

$$\frac{1}{3} \frac{\mathrm{d}^2 p}{\mathrm{d}x^2} = \mathcal{D}\kappa(x)\,(p - \phi_w)\,. \tag{17}$$

Boundary conditions (15e) and (15f) translate to conditions on the pressure,

$$\left.\frac{\mathrm{d}p}{\mathrm{d}x}\right|_{x=0} = -3\mathrm{Pe}\mathcal{D}, \tag{18a}$$

$$p(1) = 0 \tag{18b}$$

and for convenience we restate the governing equation for ϕ,

$$\mathrm{Pe}\left(u\frac{\partial \phi}{\partial x} + v\frac{\partial \phi}{\partial y}\right) = \frac{\partial^2 \phi}{\partial y^2}, \tag{19}$$

with boundary conditions

$$\left.\frac{\partial \phi}{\partial y}\right|_{y=0} = 0, \tag{20a}$$

$$\mathrm{Pe}\,\mathcal{V}\,\phi - \left.\frac{\partial \phi}{\partial y}\right|_{y=1} = 0, \tag{20b}$$

$$\phi(0, y) \equiv 1. \tag{20c}$$

The coupling between p and ϕ in the ODE for pressure (17) and advection–diffusion equation for ϕ (19) makes analytical progress difficult, if not impossible. We therefore resort to numerical solution of Eqs. (17) and (19) subject to boundary conditions (18) and (20) respectively.

We normalize the amount of fluid filtered through the walls (Eq. (11)) by the influx, $2\hat{Q}$, giving the efficiency of the filtration process as

$$E = \frac{\hat{F}}{2\hat{Q}} = \frac{F}{2}, \tag{21}$$

where

$$F = 2\int_0^1 \mathcal{V}\,\mathrm{d}x. \tag{22}$$

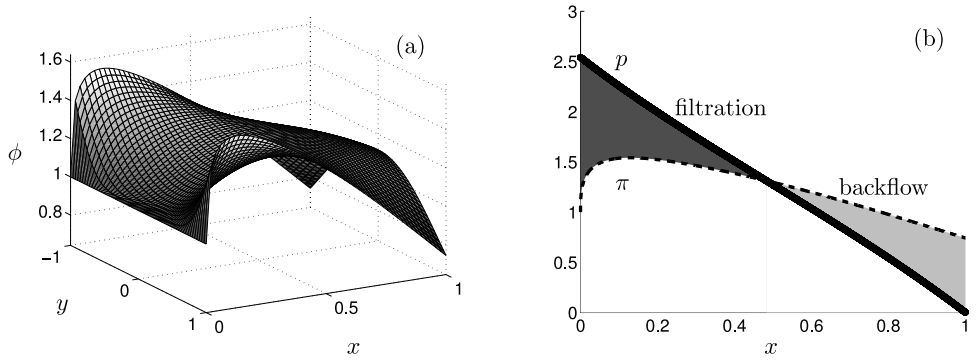

FIG. 3. (a) Particle concentration in a channel with uniformly permeable walls. Concentration polarization occurs close to the inlet but the concentration falls off with x due to concentration polarization-induced osmotic backflow and diffusion. (b) The difference in hydrodynamic pressure (solid), p, and osmotic pressure (dashed), π, determines the regions of filtration and backflow as in Eq. (15c): the dark shaded region indicates filtration; the light shaded region indicates backflow. Here, $\mathcal{D} = 1$, $\mathrm{Pe} = 1$, and $\kappa_0 = 1$.

Since the wall velocity is proportional to κ (Eq. (15c)), we expect more fluid to be filtered with larger κ. However, we consider the re-scaled efficiency, E/κ, to compare systems with different permeability.

III. UNIFORMLY PERMEABLE WALLS

We first consider a channel in which the walls are uniform with constant permeability, i.e., $\kappa(x) = \kappa_0 = \text{constant}$ for $0 \le x \le 1$. We solve the coupled pressure ODE (17) and particle advection–diffusion equation (19), subject to boundary conditions (18) and (20), numerically using a finite difference method.

Figure 3(a) shows that the system exhibits CP in the channel: ϕ increases close to the wall. In practice, CP may lead to blocking of the pores of the permeable walls, a reduced permeability of the walls, and a reduction in the proportion of water that is filtered. We do not consider this effect here, focusing instead on the effects arising further down the channel; here, CP is significantly reduced for two reasons. First, the channel loses fluid due to the permeable walls. This reduces the advection of particles and so the particles that have collected at the walls (CP) begin to diffuse away, leading to a more uniform particle distribution in the channel. Second, the osmotic pressure exceeds the hydrodynamic pressure drawing fluid into the channel from outside (Figure 3(b)).

Both CP and backflow are undesirable effects when striving to maximize filtration efficiency and so in Sec. IV we show how spatially variable permeability of the walls may mitigate these issues and increase the net filtration.

IV. A VARIABLE PERMEABILITY CHANNEL

We begin by considering a canonical example of a channel with a single region of permeable wall for $0 \le x < \lambda$ and a single region of impermeable wall for $\lambda \le x \le 1$ where $\lambda \in (0, 1)$ (Figure 1). This is motivated by the idea of blocking the permeable walls of the channel towards the end to prevent inflow (see Introduction). While we might imagine setting the permeability to be constant in the permeable region and zero in the impermeable region, the discontinuity in κ results in a discontinuity in the second derivative of the pressure and thus in the transverse flow velocity, v (Eqs. (17) and (16b), respectively). This affects the advection–diffusion of the particles via the no-flux boundary condition (20b). In reality, this discontinuity could be absorbed by revisiting our neglection of $O(\delta)$ terms but this is not particularly enlightening for our analysis. Instead, we choose a functional form for the permeability that rapidly but smoothly varies between the permeable and impermeable regions,

$$\kappa(x) = \kappa_0 \tanh\left(A\,x\right) \tanh\left[A\,(\lambda - x)\right] \theta(\lambda - x), \tag{23}$$

where κ_0 and A are constants representing the unblocked permeability and the width of the transition region, respectively, and θ is the Heaviside function. It is this value of κ_0 that we vary to analyse the dependence on the permeability. Here, we take $A = 500$ to provide a close approximation to a step function while allowing our numerical scheme to resolve the rapid variations in x.

A. λ and κ_0–dependency

Here, we fix the Péclet number, Pe = 1, and vary the strength of the permeability, κ_0, and the fraction of permeable wall region, λ. We numerically solve the coupled pressure ODE (17) and the particle advection–diffusion equation (19), subject to boundary conditions (18) and (20), using finite differences, with κ given by (23).

As in the case of the uniformly permeable channel, the particle concentration, ϕ, exhibits CP in the permeable region $x < \lambda$ (Figure 4(a)). Also, as was seen in the uniformly permeable channel case, the flow is reduced in the channel by loss of fluid through the membrane: diffusion then acts to smooth out the CP further down the channel.

In the impermeable region $x \geq \lambda$, the particles are able to diffuse back to an approximately uniform distribution across the channel (though with a higher concentration than at the origin, Eq. (20c), because of the flow of fluid through the permeable walls). The distribution becomes uniform because the transverse velocity disappears, due to the impermeable walls, and advection–diffusion equation for the particle distribution, Eq. (19), becomes a diffusion equation with zero-flux boundary conditions.

The choice of λ may significantly affect the net flux filtered through the permeable walls, F (compare Figures 3(b) and 4(b)). If λ is close to unity, then the backflow region is significant, reducing the net flux through the permeable wall. However, if λ is too small, then we reduce the region available for filtration. There is, therefore, a critical (optimal) value, $\lambda = \lambda^*$, that maximizes the efficiency of filtration, E (21), found by a numerical search of λ (Figure 5(a)).

We have observed, though not shown here, that an increase in the wall permeability increases the transport of fluid through the wall. As such, the accumulation of particles at the wall (CP) increases as well. The resulting increase in osmotic pressure leads to backflow occurring closer to the entrance of the channel. The optimal fraction of permeable wall, λ^*, thus decreases with κ_0, as does the optimal re-scaled efficiency, E^*/κ_0, as seen in Figures 5(b) and 5(c). Here, we use the previously mentioned re-scaled efficiency, E^*/κ_0, to compare the systems, however, now scaled with the maximum permeability, κ_0. Hence, the decrease in E^*/κ_0 with κ_0 is attributed to the larger osmotic pressure that occurs when more particles are advected to the wall.

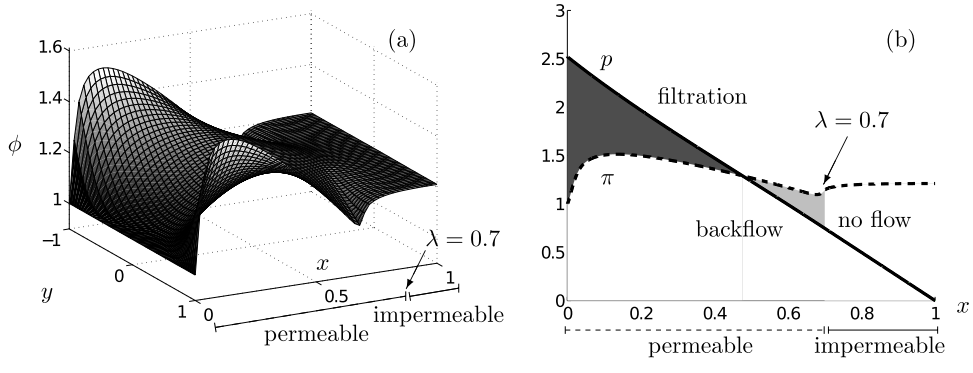

FIG. 4. (a) Particle concentration in a channel with permeable walls of varying permeability (23) with $\lambda = 0.7$. Concentration polarization in the permeable region and diffusion to a uniform concentration occurs in the impermeable region. (b) The difference in hydrodynamic (solid), p, and osmotic (dashed), π, pressures determines the regions of filtration and backflow. The dark shaded region indicates filtration, the light shaded region indicates backflow, and there is no flow in the white region between p and π. Here, $\mathcal{D} = 1$, Pe = 1, and $\kappa_0 = 1$.

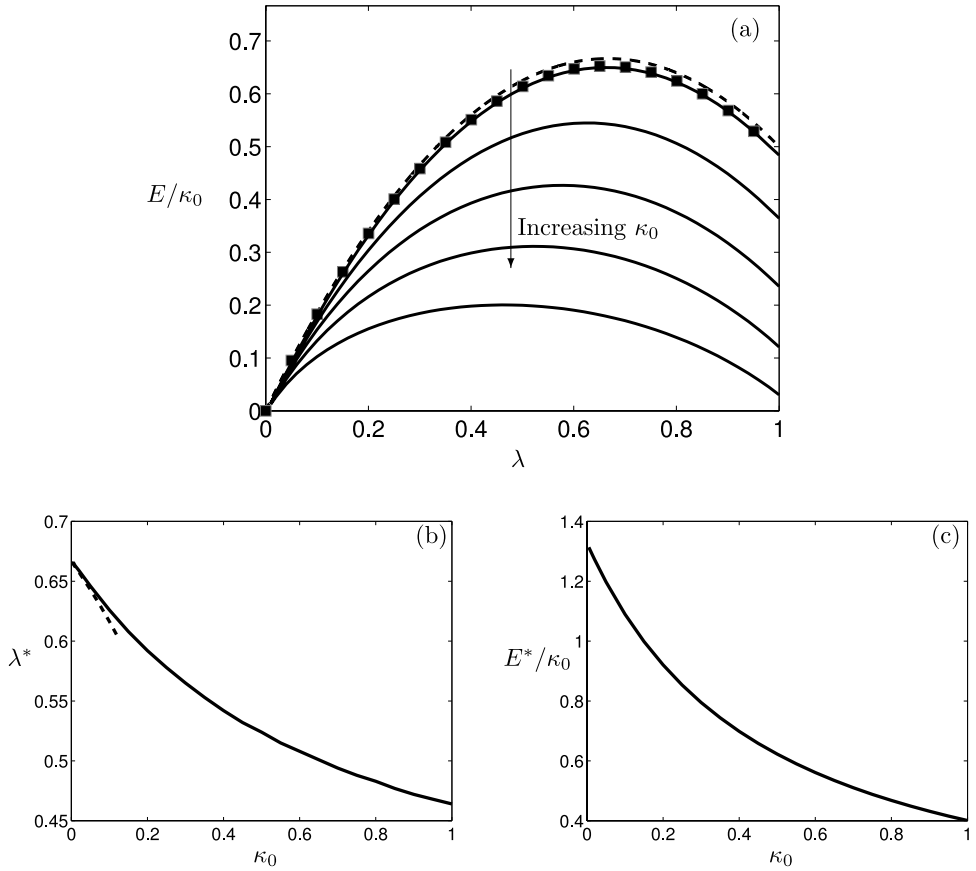

FIG. 5. (a) Dependence of re-scaled efficiency of filtration through the permeable walls, E/κ_0, on the permeable fraction of the wall, λ, for $\kappa_0 = \{0.01, 0.1, 0.25, 0.5, 1\}$ (solid curves). The dashed black curve and the squares show, respectively, leading-order and first-order asymptotic results (28), for $\kappa_0 = 0.01$. E/κ_0 is maximized by an optimal value of $\lambda = \lambda^*$; and E/κ_0 decreases with increasing κ_0. (b) The optimal permeable wall fraction, λ^*, that maximizes the efficiency of filtration, E/κ_0, of clean water out versus wall permeability, κ_0. The asymptotic result, to order-κ_0 (dashed line), for this decreasing function, matches the numerics for $\kappa_0 \ll 0.01$. (c) The re-scaled optimal efficiency, the efficiency at the optimal λ for each κ_0. Here, $\mathrm{Pe} = 1$ and $\mathcal{D} = 1$.

B. Asymptotics for small permeability

The numerical results in Sec. IV A give an insight into the behaviour of our system. We now seek to gain a deeper understanding by finding analytical expressions for the parameter dependencies in the asymptotic regime of small permeability, $\kappa_0 \ll 1$. This corresponds to a cross-flow filtration system with a very small filtration velocity. While this is less relevant to filtration applications, it gives insight into the qualitative behaviour of the system that holds even at higher permeabilities.

When the channel walls are impermeable ($\kappa_0 = 0$), flow in the channel (17) is given by a constant pressure gradient, $\mathrm{d}p/\mathrm{d}x = -3\mathrm{Pe}\mathcal{D}$ by Eq. (18a), and so the velocities in Eq. (16) read, $u = 3(1 - y^2)/2 \equiv u_0$ and $v = 0$ (i.e., Poiseuille flow). By (19), the volume fraction then remains uniform throughout, $\phi \equiv 1$. We consider the small-permeability limit, $\kappa_0 \ll 1$, as a perturbation of this uniform, unidirectional flow state with the aim of understanding the general shape shown in Figure 5(a). We perturb the variables as follows:

$$p = p_0 + \kappa_0\, p_1, \tag{24a}$$

$$u = u_0 + \kappa_0\, u_1, \tag{24b}$$

$$v = \kappa_0\, v_1, \tag{24c}$$

$$\phi = 1 + \kappa_0 \phi_1, \tag{24d}$$

$$\pi = 1 + \kappa_0 \phi_1(y = 1), \tag{24e}$$

where (24e) is obtained from Eq. (14). Equation (17) at leading and first order gives

$$\frac{\mathrm{d}^2 p_0}{\mathrm{d}x^2} = 0, \tag{25a}$$

$$\frac{\mathrm{d}^2 p_1}{\mathrm{d}x^2} - 3\mathcal{D} p_0 + 3\mathcal{D} = 0, \tag{25b}$$

respectively. Equations (25a) and (25b) must be solved subject to the boundary conditions

$$\left.\frac{\partial p_0}{\partial x}\right|_{x=0} = -3\mathrm{Pe}\mathcal{D}, \tag{26a}$$

$$p_0(1) = 0, \tag{26b}$$

$$\left.\frac{\partial p_1}{\partial x}\right|_{x=0} = 0, \tag{26c}$$

$$p_1(1) = 0, \tag{26d}$$

using Eq. (18), which gives

$$p_0 = 3\mathrm{Pe}\mathcal{D}\,(1 - x)\,, \tag{27a}$$

$$p_1 = -\frac{3}{2}\mathcal{D}\left[\mathrm{Pe}\mathcal{D}x^3 + (1 - 3\mathrm{Pe}\mathcal{D})x^2 + 2\mathrm{Pe}\mathcal{D} - 1\right]. \tag{27b}$$

The filtration efficiency, (21), is given as a function of λ by

$$E = \frac{\kappa_0 \lambda}{\mathrm{Pe}}\left(3\mathrm{Pe}\mathcal{D} - 1 - \frac{3\mathrm{Pe}\mathcal{D}\,\lambda}{2}\right) + \frac{\kappa_0^2}{\mathrm{Pe}}\int_0^\lambda (p_1 - \pi_1)\,\mathrm{d}x. \tag{28}$$

The first term in Eq. (28) (proportional to κ_0) explains the quadratic dependence on λ observed in the efficiency of filtration (Figure 5(a)). As such, the leading-order efficiency of filtration is

$$\frac{E_0}{\kappa_0} = \lambda\left(3\mathcal{D} - \frac{1}{\mathrm{Pe}} - \frac{3\mathcal{D}\,\lambda}{2}\right), \tag{29}$$

which is shown as the dashed curve in Figure 5(a). The value of λ that maximizes E_0 is then, to leading order,

$$\lambda^*_{\mathrm{asymp}} = 1 - \frac{1}{3\mathrm{Pe}\mathcal{D}}. \tag{30}$$

The order-κ_0 result may be calculated numerically and matches the result in Figure 5(b) for $\kappa_0 = 0.01$.

The osmotic term $\pi_1 = \phi_1$ that appears in (28) is determined by substituting the perturbation (24d) into the advection–diffusion equation (19) and the boundary conditions (20). The resulting $O(\kappa)$ equations are

$$\frac{\partial \phi_1}{\partial x} = \frac{2}{3\,\mathrm{Pe}\,(1 - y^2)}\frac{\partial^2 \phi_1}{\partial y^2}, \tag{31a}$$

$$\frac{\partial \phi_1}{\partial y} = 0, \qquad \text{on} \quad y = 0, \tag{31b}$$

$$\mathrm{Pe}\, v_1 - \frac{\partial \phi_1}{\partial y} = 0, \qquad \text{on} \quad y = 1, \tag{31c}$$

$$\phi_1 = 0, \qquad \text{at} \quad x = 0. \tag{31d}$$

These equations for ϕ_1 may in principle be solved by separation of variables. However, the resulting parabolic cylinder functions are complicated and do not give much insight to the solution. We therefore solve the problem numerically. The efficiency of filtration, E, can now be calculated

from (28) for various values of λ. The order-κ flux captures the shape of E as a function of λ (Figure 5(a)). Including the $O(\kappa_0^2)$ correction provides an almost indiscernible result from the full numerical solution when $\kappa_0 = 0.01$.

C. λ and Pe–dependency

The permeability is a structural part of the membrane filtration device that plays an important role in filtration; once the device is made, it cannot easily be changed. However, the Péclet number, $\mathrm{Pe} = \delta\hat{Q}/D$, is dependent on the flow rate which may easily be adjusted by the pump used in a device. This parameter is important for the transport of particles in the flow and hence heavily influences the osmotic pressure. By varying the Péclet number, we are not considering changes to the particles, e.g., radius. It is the influx that is being changed, not the diffusivity.

To investigate the role of Pe, we solve the coupled pressure ODE (17) and particle advection–diffusion equation (19), subject to boundary conditions (18) and (20), numerically using finite differences. The wall permeability, κ, is again given by (23) with $\kappa_0 = 1$ and the Péclet number is varied, together with λ. In Sec. IV A, we observed an optimal value, λ^*, for the efficiency of filtration (Figure 5(a)), that decreases with κ_0 (Figure 5(b)). We now observe a similar behaviour, i.e., the presence of an optimal value for the efficiency of filtration as we vary the Péclet number. As we increase Pe, the optimal value, λ^*, increases (Figure 6(a)), i.e., a larger fraction of permeable wall maximizes the efficiency of filtration. This can be explained by considering the pressure in the channel: the pressure gradient at the entrance is dependent on the flux, and hence on Pe (18a), resulting in greater pressures in the channel as we increase Pe. The value of λ^* asymptotes as $\mathrm{Pe} \to \infty$ because backflow is inevitable at the end of the channel since the hydrodynamic pressure vanishes (18b).

The optimal filtration efficiencies, E^*, corresponding to the optimal fraction of permeable wall, λ^*, as Pe varies also exhibits an optimum (Figure 6(b)). This provides the global maximum efficiency for both λ and Pe. This may be explained by considering the particle distribution in the channel; as we begin to increase the Péclet number, advection is dominating, however, a boundary layer at the wall exists when $\mathrm{Pe} \gg 1$. This boundary layer produces larger particle concentrations and concentration gradients at the walls, which leads to a large osmotic pressure that increases further with Pe. This competes with the large pressure in the channel and a turning point occurs, reducing the efficiency, and thus leading to an optimum.

D. Energy

We have analysed the efficiency of a filtration device composed of a region of permeable wall followed by an impermeable-walled region. However, filtration efficiency does not necessarily imply energy efficiency. In a filtration setup, the power requirement for a feed pump scales

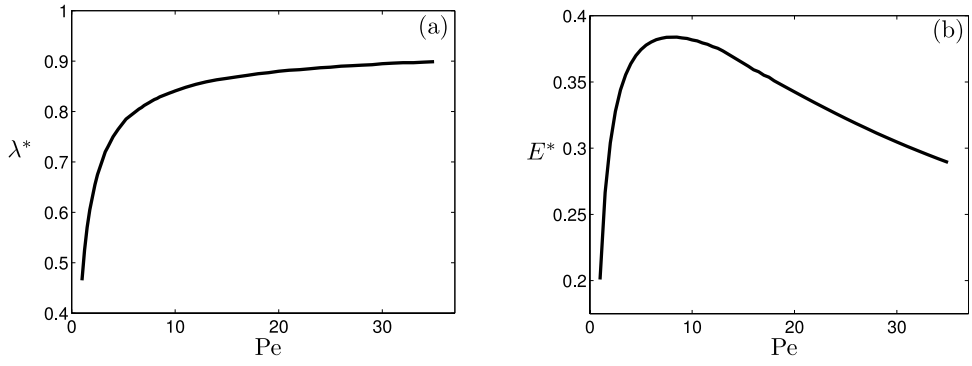

FIG. 6. (a) The optimal permeable wall fraction, λ^*, as a function of the Péclet number, Pe, increases rapidly for $\mathrm{Pe} \lesssim 10$ and asymptotes for larger values. (b) The optimal flux, E^*, corresponding to the optimal fraction of permeable wall, λ^*, for each Pe, results in a global optimal result that maximizes filtration. Here, $\kappa_0 = 1$ and $\mathcal{D} = 1$.

like $\hat{P} = \hat{Q}\,(\hat{p}(0) - \hat{p}(L))\,/e$[17,29] where $\hat{Q}$ is the influx, $\hat{p}(0) - \hat{p}(L)$ is the pressure difference in the channel, and e is the pump efficiency (a constant for a given pump). Since power corresponds to the quantity of energy ($\hat{T}$) consumed per unit time, we equate the energy with the power multiplied by the time taken to filter an areal volume, V, of fluid, $\hat{t}_f = V/\hat{Q}E$, giving

$$\hat{T} = \hat{P}\hat{t}_f = \frac{[\hat{p}(0) - \hat{p}(L)]\,V}{Ee}. \tag{32}$$

In dimensionless form, scaling $\hat{T} = (\Pi\Phi_0 V/e)T$, the energy cost (input) required for filtration scales like

$$T \sim \frac{p(0) - p(1)}{E} = \frac{p(0)}{E}, \tag{33}$$

since, in our case, $p(1) = 0$. This is a balance between how hard we push the fluid (pressure difference applied) and the filtration efficiency, E. The harder we push and/or the less efficient the system, the more energy that is consumed to filter a given amount of fluid.

The Péclet number plays an important role in the energy cost of the system, directly affecting the pressure (Eq. (18a)) and velocity (Eq. (16)) of the fluid. For any given variable-permeability channel with a permeable-region fraction, λ, an optimal value for the Péclet number, Pe*, exists that minimizes the energy expended (Figure 7(a)). This optimal value increases with λ, indicating that channels that comprise a higher fraction of permeable-wall region must operate at higher Péclet numbers to minimize energy cost (Figure 7(b)). Finally, an optimum value of λ (using the

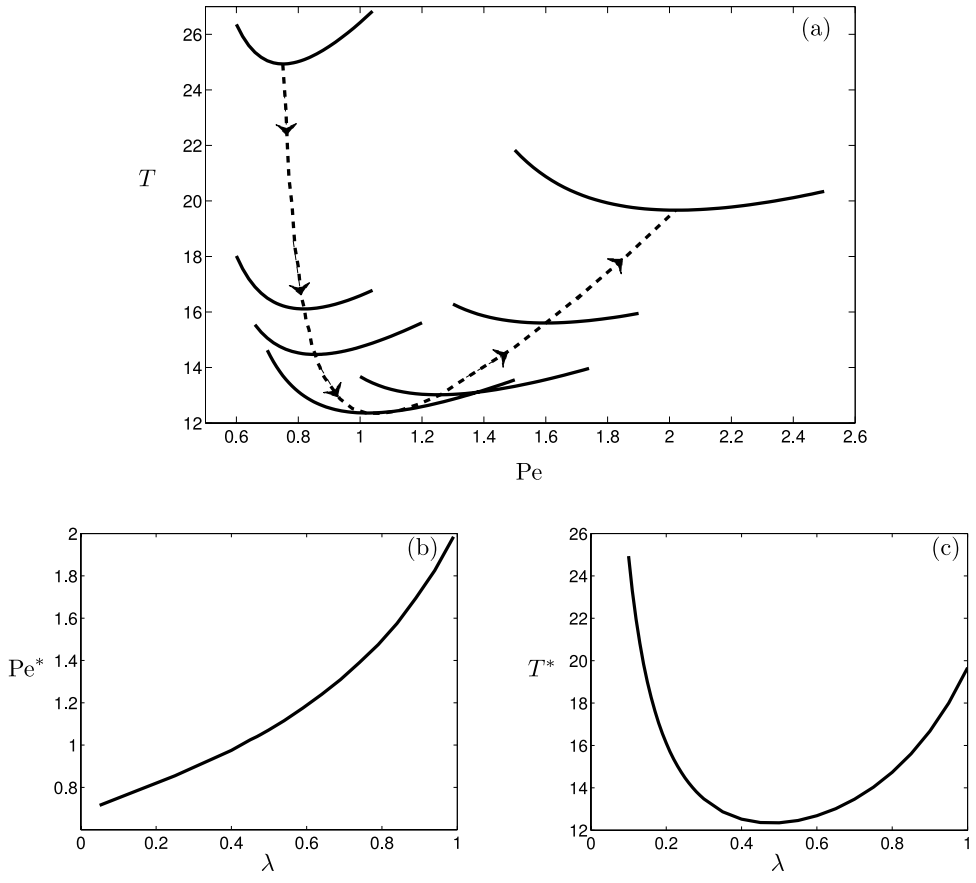

FIG. 7. (a) The energy T varies with Péclet number Pe for $\lambda = 0.1, 0.2, 0.25, 0.45, 0.65, 0.85, 1$ (solid curves with λ increasing in the direction of the arrows) giving an optimal value (dashed line) for each value of λ. (b) The Péclet number that minimizes the energy cost, Pe*, increases with λ. (c) The minimal energy cost, T^*, for each λ evaluated at the optimal Péclet number from (b) showing a global minimum. In all cases, $\kappa_0 = 1$ and $\mathcal{D} = 1$.

corresponding Pe^*) exists for which the energy is globally minimized (Figure 7(c)). This is also seen as the dashed line in Figure 7(a). When $\kappa_0 = 1$, we find that the global optimal operating conditions are $\lambda \approx 0.5$ and $Pe \approx 1.05$ (Figures 7(b) and 7(c)). We note that this optimization can yield significant advantages with, for instance, an energy saving of up to 50% when operating in this optimal regime when compared to a setup with $\lambda = 0.1$ (Figure 7(c)).

V. CONCLUSIONS

In this paper, we have explored the idea of tailoring the wall permeability in a permeable channel to optimize the amount of fluid that is filtered, addressing deleterious problems in filtration such as backflow due to osmosis and energy cost for the case where the outlet pressure is the same as the permeate side pressure. We consider the early stages of particle build-up in which filtration is compromised by an osmotic pressure opposing the filtration process. Further study is required to address later-stage mechanisms such as deposition and cake formation.

We introduced a channel with walls composed of permeable and impermeable regions. An optimum permeable wall fraction that maximizes the net flux of fluid filtered at the walls is found. This optimum arises as a result of the competing effects of hydrodynamic pressure, allowing filtration, and osmosis, causing a flow of the filtered fluid back into the channel. The optimum is a design parameter that is a decreasing function of the permeability; this indicates that setups composed of walls with higher permeability are optimized with smaller permeable regions. This is due to larger permeability resulting in larger filtration velocities, inducing a greater transport of particles to the wall and thus causing osmotic backflow to occur earlier in the channel. Our numerical results match an asymptotic result for small wall permeabilities.

Similar optima are found when varying the Péclet number. However, here the optimal permeable wall fraction increases with the Péclet number, due to the dependence of the pressure on this parameter, until an asymptote occurs due to the inevitable backflow at the end of the channel. An optimal Péclet number that maximizes filtration efficiency exists due to a boundary layer at the wall that increases the osmotic pressure.

We considered the effect of Péclet number on the energy cost of filtration and found that, given a certain fraction of permeable wall, an optimal value for the Péclet number exists that minimizes the energy to filter a given quantity of liquid. Furthermore, that optimal Péclet number increases with the fraction of the wall that is permeable and, given this, an optimal fraction of permeable wall exists that minimizes the energy.

As stated, the model presented is suitable for the early stages in a filtration process, before caking, blocking, and fouling occur. By increasing the efficiency of the filtration process at this stage, we expect this to have favourable repercussions later on in the process by significantly reducing the volume of fluid to be filtered at higher pressures.

The ideas presented here give an insight into potential methods to optimize processes in water filtration, in this case, to maximize the filtration rate for a fixed influx. We show that changes in design can greatly improve performance by minimizing energy cost and adverse effects such as backflow due to osmosis, and the results may suggest developments for the filtration industry.

ACKNOWLEDGMENTS

J. G. H. acknowledges the Bracken Bequest for support during work on this publication. The authors would like to thank C. J. W. Breward for his suggestions on an earlier version of the manuscript.

[1] W. R. Bowen and F. Jenner, "Theoretical descriptions of membrane filtration of colloids and fine particles: An assessment and review," Adv. Colloid Interface Sci. **56**, 141–200 (1995).
[2] R. H. Davis, "Modelling of fouling of crossflow microfiltration membranes," Sep. Purif. Methods **21**, 75–126 (1992).
[3] A. L. Zydney, "Stagnant film model for concentration polarization in membrane systems," J. Membr. Sci. **130**(1), 275–281 (1997).
[4] S. S. Vasan and R. W. Field, "On maintaining consistency between the film model and the profile of the concentration polarisation layer," J. Membr. Sci. **279**(1), 434–438 (2006).

[5] L. Song and M. Elimelech, "Theory of concentration polarization in crossflow filtration," J. Chem. Soc., Faraday Trans. **91**, 3389–3398 (1995).
[6] E. M. V. Hoek, A. S. Kim, and M. Elimelech, "Influence of crossflow membrane filter geometry and shear rate on colloidal fouling in reverse osmosis and nanofiltration separations," Environ. Eng. Sci. **19**(6), 357–372 (2002).
[7] R. H. Davis and J. D. Sherwood, "A similarity solution for steady-state crossflow microfiltration," Chem. Eng. Sci. **45**, 3203–3209 (1990).
[8] S. De, S. Bhattacharjee, A. Sharma, and P. K. Battacharya, "Generalized integral and similarity solutions of the concentration profiles for osmotic pressure controlled ultrafiltration," J. Membr. Sci. **130**, 99–121 (1997).
[9] P. Bacchin, D. Si-Hassen, V. Starov, M. J. Clifton, and P. Aimar, "A unifying model for concentration polarization, gel-layer formation and particle deposition in cross-flow membrane filtration of colloidal suspensions," Chem. Eng. Sci. **57**, 77–91 (2002).
[10] B. J. Bellhouse and R. W. H. Lewis, "A high efficiency membrane separator for donor plasmapheresis," ASAIO J. **34**(3), 747–754 (1988).
[11] R. J. Wakeman and C. J. Williams, "Additional techniques to improve microfiltration," Sep. Purif. Technol. **26**(1), 3–18 (2002).
[12] N. Hilal, O. O. Ogunbiyi, N. J. Miles, and R. Nigmatullin, "Methods employed for control of fouling in MF and UF membranes: A comprehensive review," Sep. Sci. Technol. **40**(10), 1957–2005 (2005).
[13] R. W. Field and G. K. Pearce, "Critical, sustainable and threshold fluxes for membrane filtration with water industry applications," Adv. Colloid Interface Sci. **164**, 38–44 (2011).
[14] O. Kedem and A. Katchalsky, "Thermodynamic analysis of the permeability of biological membranes to non-electrolytes," Biochim. Biophys. Acta **27**, 229–246 (1957).
[15] J. G. Wijmans and R. W. Baker, "The solution-diffusion model: A review," J. Membr. Sci. **107**, 1–21 (1995).
[16] J. G. Herterich, I. M. Griffiths, R. W. Field, and D. Vella, "The effect of a concentration-dependent viscosity on particle transport in a channel flow with porous walls," AIChE J. **60**, 1891 (2014).
[17] W. Xi and S. Geissen, "Separation of titanium dioxide from photocatalytically treated water by cross-flow microfiltration," Water Res. **35**(5), 1256–1262 (2001).
[18] G. K. Batchelor, "Brownian diffusion of particles with hydrodynamic interaction," J. Fluid Mech. **74**, 1–29 (1976).
[19] A. J. DiLeo, A. E. Allegrezza, and S. E. Builder, "High resolution removal of virus from protein solutions using a membrane of unique structure," Nat. Biotechnol. **10**(2), 182–188 (1992).
[20] A. Gabelman and S.-T. Hwang, "Hollow fiber membrane contactors," J. Membr. Sci. **159**(1), 61–106 (1999).
[21] É. Guazzelli and J. F. Morris, *A Physical Introduction to Suspension Dynamics* (Cambridge University Press, 2012).
[22] M. Amiji and B. Sandmann, *Applied Physical Pharmacy* (McGraw Hill Professional, 2003).
[23] E. F. Casassa and H. Markovitz, "Statistical thermodynamics of polymer solutions. I. Theory of the second virial coefficient for a homogeneous solute," J. Chem. Phys. **29**(3), 493–503 (2004).
[24] G. S. Beavers and D. D. Joseph, "Boundary conditions at a naturally permeable wall," J. Fluid Mech. **30**, 197–207 (1967).
[25] F. W. Altena and G. Belfort, "Lateral migration of spherical particles in porous flow channels: Application to membrane filtration," Chem. Eng. Sci. **39**(2), 343–355 (1984).
[26] R. J. Shipley, S. L. Waters, and M. J. Ellis, "Definition and validation of operating equations for poly(vinyl alcohol)-poly(lactide-co-glycolide) microfiltration membrane-scaffold bioreactors," Biotechnol. Bioeng. **107**, 382–392 (2010).
[27] W. R. Bowen and P. M. Williams, "Prediction of the rate of cross-flow ultrafiltration of colloids with concentration-dependent diffusion coefficient and viscosity—Theory and experiment," Chem. Eng. Sci. **56**, 3083–3099 (2001).
[28] R. F. Probstein, *Physicochemical Hydrodynamics. An Introduction* (Butterworths, 1989).
[29] K. Parameshwaran, A. G. Fane, B. D. Cho, and K. J. Kim, "Analysis of microfiltration performance with constant flux processing of secondary effluent," Water Res. **35**(18), 4349–4358 (2001).
[30] Y Wang, JA Howell, RW Field, and MR Mackley, "Oscillatory flow within porous tubes containing wall or central baffles," Trans IChemE **72**, Part A 686-694 (1994).